Characterization of the Reaction Products of Laser-Ablated Late Lanthanide Metal Atoms with Molecular Oxygen: Infrared Spectra of LnO, LnO^+, LnO^-, LnO_2, LnO_2^-, LnO_3^-, and $(LnO)_2$ in Solid Argon

Stephen P. Willson and Lester Andrews*

Chemistry Department, University of Virginia, Charlottesville, Virginia 22901

Received: April 26, 1999; In Final Form: June 29, 1999

This paper is the second segment of an investigation into the reaction products of laser-ablated lanthanide metal atoms with O_2. There is general agreement with previous gas-phase and matrix infrared observations of neutral lanthanide monoxides; the frequencies of monoxide cations and anions are original to this work. The dioxide anion vibrational frequencies of all late lanthanides and neutral frequencies of five of the last seven are reported. In conjunction with the earlier part of this study, it is found that the average vibrational frequencies of the early lanthanide dioxide anions are lower than their neutral counterparts, while those of the late lanthanide dioxide anions are higher. Doping the electron scavenger, CCl_4, into these samples provides a diagnostic test for the identification of molecular cations and anions by matrix infrared spectroscopy.

Introduction

The available experimental and theoretical literature pertaining to the lanthanide monoxide molecules is extensive.[1−22] Gas-phase assignments of the ground electronic states have been made for all of the neutral lanthanide monoxides except TmO, for which the vibrational frequency of the matrix-isolated species has been reported.[13] There have also been identifications of several neutral lanthanide dioxides in rare gas matrices[13,14,16] and of dioxide cations in mass spectrometry observations.[23−26] Chemielectron spectroscopy has determined that most lanthanide monoxide cations and two dioxide cations form spontaneously upon reaction of atomic lanthanide metals with molecular oxygen.[27]

The current report continues a recent study of the reaction products of laser-ablated early lanthanide metal atoms with O_2.[28] Infrared spectra of the matrix isolated reaction products provide substantial evidence for the monoxide cations, neutrals, and anions as well as the dioxide neutrals and anions for the latter half of the lanthanide series. Together with the previous paper, a complete picture is provided of the monoxide and dioxide vibrational frequencies and their anions. Several trends are identified for these species within the lanthanide series.

Experimental Section

Lanthanide metal atoms supplied by laser vaporization were reacted with molecular oxygen in argon matrices using techniques described in previous publications.[29−32] Experiments required O_2/Ar concentrations ranging from 0.5% to 3% deposited at a rate of 4−5 mmol/h for 1−3 h onto a CsI window held at 6−7 or 10−11 K. Samples of $^{18}O_2$, mixed $^{16}O_2 + {}^{18}O_2$, and scrambled $^{16}O_2 + {}^{16}O^{18}O + {}^{18}O_2$ were also employed. To identify charged products, some gas sample mixtures were doped with CCl_4, not exceeding 10% of the total O_2 concentration in the sample. Complementary neon experiments were done for Dy and Ho with concentrations of 0.2−0.5% O_2 deposited at 6−7 K. Infrared spectra were recorded at 0.5 cm^{-1} resolution with a Nicolet 750, 550, or 60SXR spectrometer after deposition and after each annealing or photolysis. The peak positions are measured to 0.1 cm^{-1} accuracy, and isotopic frequency ratios are calculated to ±0.0004.

The metal targets, Tb, Dy, Ho, Er, Tm, Yb, and Lu (all Johnson-Matthey 99.9%), were ablated with the 1064 nm fundamental of a YAG laser, typically with 5−50 mJ pulses. For low laser power experiments, a 10% transmitting neutral density filter was placed in the laser beam. Under these conditions, measurement of the metal volume ablated (laser groove) allows an estimate of the matrix/metal ratio of 1000:1. Clearly, O_2 is in considerable excess. Following deposition, argon matrixes were annealed to 25 K, then subjected to photolysis (240−580 nm) using a 175 W mercury street lamp (Philips H39KB) without the globe. Alternately, matrices were subjected to a series of photolyses beginning with a tungsten lamp, with glass filters, and finally with the mercury arc lamp. Annealing cycles raise the matrix temperature to the specified value, then cool back to the deposition temperature. Further annealings were done after photolysis and additional spectra were recorded.

Results

Infrared absorptions for laser-ablated lanthanide metal atom, cation, and electron reactions with dioxygen fall into two broad categories, those identified as O−O vibrations and those due to Ln−O modes. Oxygen−oxygen vibrations observed range from perturbed O_2 near 1552 cm^{-1} to O_3^- at 804 cm^{-1} in solid argon and include O_4^+ at 1118.6 cm^{-1}, O_3 at 1039.6 and 1033.1 cm^{-1}, and O_4^- at 953.7 cm^{-1};[33−37] these bands, found for all metals, are listed only in Table 1. The metal−oxygen fundamentals range from 450 to 900 cm^{-1}, and absorption bands for each metal are listed with their $^{18}O_2$ isotopic counterparts and annealing behavior in Tables 1−7; differences observed after photolysis or with the doping of samples with the electron scavenger, CCl_4, are also included with the annealing data. For Dy and Ho, neon observations are listed below the argon results in the same table. Examples of important spectral regions are provided in Figures 1−6 for clarification of the text.

Calculations

Theoretical calculations were performed for several lanthanide monoxide species with the Amsterdam Density Functional (ADF

10.1021/jp991338m CCC: $18.00
Published on Web 08/13/1999

TABLE 1: Product Absorptions (cm^{-1}) Observed for Laser-Ablated Tb Atoms with O_2 in Solid Argon at 10 K

$^{16}O_2$	$^{18}O_2$	$^{16}O_2 + {}^{18}O_2$	$^{16}O_2 + {}^{16}O^{18}O + {}^{18}O_2$	$R(16/18)$[a]	anneal.[b]	identity
1554.6	1466.8		1554, 1511, 1466	1.0599	b+	$(OO)Tb_x$
1510.9	1431.9		1511.0, 1484.1, 1432.0	1.0552	a+ −	TbO_2 $2\nu_1$
1467.0	1392.9	1467.0, 1392.9	1467.0, 1435.5, 1392.9	1.0532	a− −	TbO_2 $\nu_1 + \nu_3$ site
1465.5	1391.5	1465.5, 1391.4	1465.5, 1433.9, 1391.4	1.0532	a+ −	TbO_2 $\nu_1 + \nu_3$
1433.0	1362.5		−, −, 1362.5	1.0517	a+ −	TbO_2 $2\nu_3$
1388.3	1379.2	1388.2, 1379.2		1.0066		HO_2
1127.3	1063.7		1127.3, 1096.1, 1063.8	1.0598	a+ +(+)**	$(O_2)TbO_2$ site
1116.0	1053.1		1116.0, 1085.0, 1053.0	1.0597	b+	$(O_2)TbO_2$ site
1111.7	1049.1		1111.9, 1081.0, 1049.4	1.0597	b+	$(O_2)TbO_2$ site
1110.1	1047.4		1110.1, 1079.3, 1047.4	1.0599	a+ −(−)**	$(O_2)TbO_2$
1039.5	982.3			1.0582		O_3
1032.9	976.2			1.0581		O_3 site
953.6	901.6			1.0577		O_4^-
923.5	875.8			1.0545	a+ −(+)	?
889.1	841.6			1.0564		?
856.5	812.2	856.5, 812.2	856.4, 812.1	1.0545	a− −(+)*	TbO^+
823.9	781.4	823.9, 781.5	823.9, 781.6	1.0544	a− −(−)	TbO
820.2	777.9	820.3, 777.9	820.2, 777.9	1.0544	a− −(−)	TbO site
816.8	774.7	816.9, 774.6	816.8, 774.6	1.0543	a− −(−)	TbO site
804.4	759.9			1.0586	b+	$Tb^+O_3^-$
782.9	742.5	783.0, 742.9	783.2, 742.7	1.0544	a+ −(−)	TbO^-
758.6	718.7	758.6, (718.6)	758.6, 746.4, (718.6)	1.0555	a0−(+)	TbO_2 ν_1
752.7	713.1			1.0555	b+(−)	$(O_2)TbO_2$ ν_1
728.0	693.1	728.0, 693.1	728.1, 707.0, −	1.0504	a+ −	?
718.6	683.2	718.6, 683.1	718.6, 693.1, 683.1	1.0518	a0−(+)	TbO_2 ν_3
711.6	676.3			1.0522	b+(−)	$(O_2)TbO_2$ ν_3
711.2	673.2	711.1, 673.3	711.1, 698.6, 673.1	1.0564	a0−(−)**	TbO_2^- ν_1
669.0	636.5	669.0, 636.5	669.0, 646.1, 636.5	1.0511	a0−(−)**	TbO_2^- ν_3
638.6	605.8	638.5, −		1.0541	a+ −**	?
607.2	576.7	606.9, 592.3, 576.4	607.2, 592.6, 576.8	1.0529	a+ −(+)**	$(TbO)_2$ B_{3u}
602.4	570.9		604, 588, 572	1.0531	b+	$(OO)_x(TbO)_2$ B_{3u}
596.1	566.7	596.1, 566.7	566.6	1.0519	a− −(−)**	TbO_3^-
564.1	536.7			1.0511	a− −**	?
543.7	515.9	543.7, 515.9		1.0539	a− −(−)**	?
532.7	505.6	532.6, 515.6, 505.8	532.6, 515.7, 505.6	1.0536	a+ −(+)**	$(TbO)_2$ B_{2u}
528.3	501.5		528.3, 511.5, 501.4	1.0536	b+	$(OO)_x(TbO)_2$ B_{2u}

[a] Ratio (16/18) isotopic frequencies. [b] Annealing behavior: "a" denotes presence on deposition, "+, −, or 0" indicates the direction of growth in two successive annealings, "b" denotes appearance on the first annealing and "+, −, or 0" indicates changes on the second annealing, "+ or −" indicates changes on photolysis, "c" denotes appearance on photolysis, "*" indicates an increase with CCl_4 on deposition, and "**" indicates a decrease with CCl_4 on deposition.

TABLE 2: Product Absorptions (cm^{-1}) Observed for Laser-Ablated Dy Atoms with O_2 in Solid Argon and Neon

$^{16}O_2$	$^{18}O_2$	$^{16}O_2 + {}^{18}O_2$	$^{16}O_2 + {}^{16}O^{18}O + {}^{18}O_2$	$R(16/18)$[a]	anneal.[b]	ident.
			Argon			
1554.3	1466.6		1554.2, 1511.0, 1466.4	1.0598	b+(−)	$(OO)Dy_x$
1551.6	1463.9		1551.6, 1508.3, 1463.7	1.0599	b+(−)	$(OO)Dy_x$ site
			1210.6	1.0593	a0−(+)	DyO_2 $2\nu_1$
1189.4	1128.0	1189.4, 1128.0	1189.4, 1165.4, 1128.1	1.0544	a0−(+)	DyO_2 $\nu_1+\nu_3$
1107.8	1045.2		1107.8, 1077.0, 1045.2	1.0599	a+−	$(O_2)DyO_2$
861.2	816.5	861.3, 816.5	861.2, 816.5	1.0547	a− −(+)*	DyO^+
829.0	786.1	829.0, 786.1	829.0, 786.0	1.0546	a− −(−)	DyO
825.4	782.7	825.5, 782.3	825.4, 782.7	1.0546	a− −(−)	DyO site
821.8	779.3	821.8, 779.7	821.8, 779.5	1.0545	a− −(−)	DyO site
802	760			1.055	b+(−)	$Dy^+O_3^-$
782.0	745.1	781.8, 745.5	782.0, 745.2	1.0495	a+ −(−)**	DyO^-
693.9		693.9, −	693.8, 677.1, 656.9	1.0562	a+ −(−)**	DyO_2^- ν_1
			607.5		a0−(+)	DyO_2 ν_1
609.6	578.6	609.6, 594.9, −	609.6, 595.0, −	1.0536	a+ −(+)**	$(DyO)_2$
603.8	572.5	603.9, −		1.0547	a+ −(−)**	?
580.5	553.3	580.5, 553.3	580.4, 561.1, 553.3	1.0492	a0−(+)	DyO_2 ν_3
574.6	548.5	574.7, 548.4	574.6, 559.6, 548.4	1.0476	a+ −(−)**	DyO_2^- ν_3
535.8	509.8	535.9, 509.9		1.0510	a− −(−)**	?
522.2	495.8	522.3, 505.9, 495.9	522.1, 505.9, 495.8	1.0532	a+ −(+)**	$(DyO)_2$
495.2	470.3			1.0529	a0−	?
			Neon			
888.6	842.3			1.0550	a0−(−)	DyO^+
839.0	795.8			1.0543	a− −(−)	DyO
599.2	571.3			1.0488	a0−(+)	DyO_2 ν_3
591.2	564.1			1.0480	a− −(−)	DyO_2^- ν_3

[a] Ratio (16/18) isotopic frequencies. [b] Annealing behavior: "a" denotes presence on deposition, "+, −, or 0" indicates the direction of growth in two successive annealings, "b" denotes appearance on the first annealing and "+, −, or 0" indicates changes on the second annealing, "+ or −" indicates changes on photolysis, "c" denotes appearance on photolysis, "*" indicates an increase with CCl_4 on deposition, and "**" indicates a decrease with CCl_4 on deposition.

2.1) program developed by Baerends et al.[38−40] Exchange and correlation were accounted for using the Vosko, Wilk, and Nusair parametrized local density approximation,[41] with nonlocal exchange and correlation corrections handled by the Becke and Perdew method (BP86).[42,43] The numerical integration parameter was set to 6.0, which is expected to provide reasonably accurate

TABLE 3: Product Absorptions (cm^{-1}) Observed for Laser-Ablated Ho Atoms with O_2 in Solid Argon and Neon

$^{16}O_2$	$^{18}O_2$	$^{16}O_2 + {}^{18}O_2$	$^{16}O_2 + {}^{16}O^{18}O + {}^{18}O_2$	$R(16/18)^a$	anneal.^{b}	ident.
			Argon			
1554.0	1466.5	1554.4, 1466.6	1550, 1507, 1462	1.0597	b+(−)	$(OO)Ho_x$
1178.7	1119.1	1179, 1119		1.0533	a0−	?
1107.0	1044.6	1107.0, 1044.6		1.0597	a+ +(−)	?
860.5	816.1	860.5, 816.0	860.5, 816.0	1.0544	a− −(+)*	HoO^+
828.1	785.2	828.1, 785.2	828.1, 785.2	1.0546	a− −(−)	HoO
824.5	781.9	824.5, 781.8	824.8, 782.1	1.0545	a− −(−)	HoO site
820.9	778.4	820.9, 778.4	821.1, 778.5	1.0546	a− −(−)	HoO site
804	759			1.0593	b+(+)	$Ho^+O_3^-$
783.6	746.6	−, 746.6	−, 746.6	1.0496	a+ −(−)**	HoO^-
696.2	659.1	696.2, 659.1	696.3, 681.7, −	1.0563	a− −(−)**	HoO_2^- ν_1
649.2	613.5	649.2, 613.5	649.2, 633.5, 613.5	1.0582	a+ −(+)	HoO_2 ν_1
644.9	614.9	644.7, 614.9	644.9, 631.4, 615.0	1.0488	c−	HoO_2^+ ν_3 tentative
615.1	583.1	614.9, 583.2		1.0549	a+ −(+)	?
583.9	556.3	−, 556.4	584.0, 565.5, 556.5	1.0496	b+	$(O_2)HoO_2$ ν_3 tent.
574.3	546.3	574.5, 546.3		1.0513	a+ +(−)*	?
549	522	549, 522	549, 534, −	1.052	a+ −(+)	HoO_2 ν_3
547	520			1.052	a− −(−)**	HoO_2^- ν_3
			Neon			
1551.8	1464.0			1.0600	a0+	$(OO)_xHo_y$
1435.0	1354.9			1.0591	a0+(−)	$(OO)_xHo_y$
887.9	841.9			1.0546	a00(−)	HoO^+
838.1	794.6			1.0547	a0+	HoO
807.8	762.9			1.0589	a0+(+)	$Ho^+O_3^-$
794.6	751.8			1.0569	a0−	?
756.6	720.9			1.0495	a0+(−)	?
668.2	631.1			1.0588	a0−(+)	HoO_2 ν_1
657.9	627.6			1.0483	c0	HoO_2^+ ν_3 tentative
629.4	596.7			1.0548	a0+(+)	?

[a] Ratio (16/18) isotopic frequencies. [b] Annealing behavior: "a" denotes presence on deposition, "+, −, or 0" indicates the direction of growth in two successive annealings, "b" denotes appearance on the first annealing and "+, −, or 0" indicates changes on the second annealing, "+ or −" indicates changes on photolysis, "c" denotes appearance on photolysis, "*" indicates an increase with CCl_4 on deposition, and "**" indicates a decrease with CCl_4 on deposition.

TABLE 4: Product Absorptions (cm^{-1}) Observed for Laser-Ablated Er Atoms in Solid Argon at 10 K

$^{16}O_2$	$^{18}O_2$	$^{16}O_2 + {}^{18}O_2$	$^{16}O_2 + {}^{16}O^{18}O + {}^{18}O_2$	$R(16/18)^a$	anneal.^{b}	ident.
1554.2	1467.0	1554, 1467	1554, 1509, 1467	1.0594	b+(−)	$(OO)Er_x$
1488.9	1406.4	1489.3, 1406.3	1488.9, 1448.3, 1406.1	1.0587	a+ −(−)	?
1116.4	1053.5	1116.4, 1053.5	1116.5, 1085.5, 1053.4	1.0597	a+ +	$Er_x(O_2)$
1106.0	1043.8	1106.0, 1043.8	1106.0, 1075.3, 1043.7	1.0596	a+0(−)	$Er_x(O_2)$ site
861.8	817.0	861.7, 816.9	861.8, 816.9	1.0548	a− −(+)*	ErO^+
828.5	785.5	828.4, 785.5	828.7, −	1.0547	a− −(−)	ErO
824.9	782.1	824.9, 782.1	825.0, 782.3	1.0547	a− −(−)	ErO site
821.2	778.6	821.3, 778.7	821.3, 778.6	1.0547	a− −(−)	ErO site
803.9	759.2			1.0589	b+(−)	$Er^+O_3^-$
788.8	747.8	788.8, 747.8	788.7, 747.9	1.0548	a+ −(−)**	ErO^-
782.6	742.0	782.7, 742.1		1.0547	b−(−)	ErO^- site
766.1	723.9	766.1, 724.1	766.1, 723.7	1.0583	a+ +	?
702.3	665.0	702.4, 664.9		1.0561	a− −(−)**	ErO_2^- ν_1
675.5	639.0			1.0571	a+ −(+)*	?
613.4	583.0	613.5, 583.1		1.0521	a− −(−)**	ErO_2^- ν_3
573.7	545.5			1.0517	a0−(−)*	?

[a] Ratio (16/18) isotopic frequencies. [b] Annealing behavior: "a" denotes presence on deposition, "+, −, or 0" indicates the direction of growth in two successive annealings, "b" denotes appearance on the first annealing and "+, −, or 0" indicates changes on the second annealing, "+ or −" indicates changes on photolysis, "c" denotes appearance on photolysis, "*" indicates an increase with CCl_4 on deposition, and "**" indicates a decrease with CCl_4 on deposition.

geometries and vibrational frequencies.[40] The basis sets were triple-ζ with one polarization function included for the O atom, but without polarization functions for the Ln metal atoms (ADF 2.1, Basis Set IV). The Ln atoms were frozen through the 4d level, and the O atom was frozen through 1s. First order relativistic scalar corrections and diagonalization in the nonrelativistic basis yielded quasirelativistic solutions.[44,45] Computational results are provided in Table 8.

Discussion

The primary reaction products of laser-ablated lanthanide metal atoms with O_2 are LnO and LnO_2. The ablated metal atoms form excited dioxide insertion products, which are relaxed by the matrix or decompose to the monoxide molecules, reaction 1.

$$Ln + O_2 \rightarrow [OLnO]^* \rightarrow LnO_2 \text{ or } O + LnO \qquad (1)$$

Since metal cations and electrons are also ablated, the charge on a given metal oxide product is identified by doping reactant gas mixtures with CCl_4 to capture electrons, minimizing the formation of metal oxide anions and favoring cation reaction products.

The neutral molecules agree with previous thermal matrix isolation and gas-phase assignments for the monoxides and one of the dioxides,[1−16] which confirms that these are *monometal* product species. Furthermore, variation of laser power over a 10-fold range retains the same sharp product bands for *monometal* species; weak, broad, unlisted bands in spectra of high laser power experiments could be due to unidentified metal cluster species. In an experiment with pure dioxygen, the only products are $Ln^+O_3^-$ and O_3, again supporting the *monometal* stoichiometry of these reaction products.

This discussion is divided into sections based on molecular formula, with the ions of each metal analogue discussed in turn,

TABLE 5: Product Absorptions (cm^{-1}) Observed for Laser-Ablated Tm Atoms in Solid Argon at 10 K

$^{16}O_2$	$^{18}O_2$	$^{16}O_2 + ^{18}O_2$	$^{16}O_2 + ^{16}O^{18}O + ^{18}O_2$	$R(16/18)^a$	anneal.[b]	ident.
1554	1467		1554, 1509, 1466	1.0593	b+	$(OO)Tm_x$
1109.5	1046.8		1109.6, 1078.6, 1046.6	1.0599	b+**	$Tm_x(O_2)$ site
1103.8	1041.6		1103.7, 1073.1, 1041.4	1.0597	a+ +**	$Tm_x(O_2)$
864.2	819.3	864.3, 819.4	864.2, 819.2	1.0548	a− −(+)*	TmO^+
834.1	790.9	834.3, 791.2	834.2, —	1.0546	a− −(−)	TmO site
832.0	788.9	832.1, 789.0	832.1, 789.0	1.0546	a− −(−)	TmO
828.6	785.7	828.7, 785.8	828.6, 785.9	1.0546	a− −(−)	TmO site
824.8	782.2	824.9, 782.3	825.0, 782.4	1.0545	a− −(−)	TmO site
806.7	762.3			1.0582	a+ +	$Tm^+O_3^-$
793.2	752.0	793.3, 752.0	793.2, 752.1	1.0548	a+ −(−)	$(O_2)_xTmO$
787.2	746.3	787.2, 746.3	787.3, —	1.0548	b−	$(O_2)_xTmO$ site
766.2	724.2	766.4, 724.4	766.3, 746.1, 724.1	1.0580	a+ +(−)	?
710.5	673.6	710.5, 673.7		1.0548	a− −	?
706.6	668.9	706.5, 668.8	706.6, 691.2, 669.0	1.0564	a− −(−)	TmO_2 ν_1
615.7	585.2	615.7, 585.2	615.7, 597.2, 585.3	1.0521	a− −(−)	TmO_2 ν_3
613.1	582.9	612.9, 582.8		1.0518	a− −(−)**	TmO_2^- ν_3 tentative
596.3	565.8			1.0539	a− −(+)**	?
572.2	543.9	572.2, 543.9	572.1, 554.7, —	1.0520	a0−(−)*	?
553.7	525.1	553.7, 525.2	553.8, —, —	1.0545	a− −(−)	$(TmO)_2$
541.3	513.5	541.3, 513.4	541.4, 523.8, 513.5	1.0541	a− −(+)**	$(O_2)(TmO)_2$

[a] Ratio (16/18) isotopic frequencies. [b] Annealing behavior: "a" denotes presence on deposition, "+, −, or 0" indicates the direction of growth in two successive annealings, "b" denotes appearance on the first annealing and "+, −, or 0" indicates changes on the second annealing, "+ or −" indicates changes on photolysis, "c" denotes appearance on photolysis, "*" indicates an increase with CCl_4 on deposition, and "**" indicates a decrease with CCl_4 on deposition.

TABLE 6: Product Absorptions (cm^{-1}) Observed for Laser-Ablated Yb Atoms in Solid Argon at 10 K

$^{16}O_2$	$^{18}O_2$	$^{16}O_2 + ^{18}O_2$	$^{16}O_2 + ^{16}O^{18}O + ^{18}O_2$	$R(16/18)^a$	anneal.[b]	ident.
1550.4	1462.8	1550.1, 1462.6	1550.0, 1506.9, 1462.5	1.0599	b+	$(OO)Yb_x$
			1261.7			YbO_2 $2\nu_1$
1259.8	1194.7	1259.9, 1194.6	1260.0, 1238.2, 1194.5	1.0545	a0−(+)	YbO_2 $\nu_1 + \nu_3$
			1193 sh			YbO_2 $2\nu_3$
809	765			1.058	b+(+)	$Yb^+O_3^-$
788.7	747.8	788.7, 747.8	788.7, 747.8	1.0547	a+ +(−)	YbO^+
701.2	- - -	701.2, —	701.1, 685.2, —	—	a− −(−)**	YbO_2^- ν_1
670.2	635.4	670.3, 635.2	670.4, —	1.0548	a− −(−)	YbO site
660.0	625.8	659.9, —	660.0, 625.8	1.0547	a+0(−)	YbO
			635.0		a0−(+)	YbO_2 ν_1
627.7	597.9	627.6, 597.8	627.7, 600.7, 597.8	1.0498	a0−(+)	YbO_2 ν_3
604.2	574.6	604.4, 574.8	604.5, 586.5, 574.8	1.0515	a− −(−)**	YbO_2^- ν_3
590.9	560.6	590.8, 560.6		1.0540	a+ +(+)	$(YbO)_2$
540.1	512.3	540.0, 512.3	539.9, 523.1, 512.2	1.0543	a+0(+)	$(YbO)_2$
516.7	489.8	516.5, 489.8		1.0549	a− −(−)	?
495.4	468.7	495.3, 468.7		1.0570	a+ −(+)*	?
474.3	449.7	474.4, 449.7		1.0547	a+ −(−)	?

[a] Ratio (16/18) isotopic frequencies. [b] Annealing behavior: "a" denotes presence on deposition, "+, −, or 0" indicates the direction of growth in two successive annealings, "b" denotes appearance on the first annealing and "+, −, or 0" indicates changes on the second annealing, "+ or −" indicates changes on photolysis, "c" denotes appearance on photolysis, "*" indicates an increase with CCl_4 on deposition, and "**" indicates a decrease with CCl_4 on deposition.

and oxygen-16 frequencies provided with oxygen-18 counterparts in parentheses. For the purpose of this discussion, the term "mixed oxygen" refers to $^{16}O_2 + ^{18}O_2$ in 1:1 proportion and the term "scrambled oxygen" refers to $^{16}O_2 + ^{16}O^{18}O + ^{18}O_2$ in 1:2:1 proportion.

Monoxides. All late lanthanide oxide systems provided neutral monoxides and singly charged monoxide cations, and four produced singly charged anions. An overall picture of the lanthanide monoxide series, except for Eu and Yb, is provided in Figure 1. Tm and Lu yielded an oxygen complexed neutral monoxide instead of the monoxide anion, which is reasonable since La does the same.[46] Identification of monoxide species is dependent on both the oxygen isotopic frequency ratio and on the number of corresponding peaks in isotopically scrambled oxygen samples. Oxygen isotopic ratios are in close agreement with the harmonic LnO ratios, and the scrambled oxygen isotopic samples provide doublets, indicating the motion of exactly one oxygen atom in the observed vibrations. Doping with CCl_4 increased cation and decreased anion absorptions relative to neutral molecule absorption intensities, which arise because ablated electrons are effectively trapped by CCl_4.[28,47]

As with the early lanthanide monoxides, several paths are instrumental in the formation of ions.[28] Chemiionization reaction 2 is predicted to be spontaneous for Ln = Tb, Dy, Ho, Er, and perhaps Lu.[27] Reaction 3 likely occurs, as metal cations are also produced by laser vaporization of the metals. It appears that matrix condensation stabilizes LnO_2 more effectively than LnO_2^+. Photoionization reaction 4 is observed for some matrix isolated molecules, although not for LuO, which has an ionization potential that is too large for the Hg arc to attain, even with matrix stabilization. Anions are formed by electron capture reaction 5, and tungsten lamp photolysis increases LnO^- absorptions using electrons produced in the matrix from the destruction of O_4^-.[48]

$$Ln + O \rightarrow LnO^+ + e^- \quad (2)$$

$$Ln^+ + O_2 \rightarrow [OLnO]^{+*} \rightarrow LnO_2^+ \text{ or } O + LnO^+ \quad (3)$$

$$LnO + h\nu \rightarrow LnO^+ + e^- \quad (4)$$

$$LnO + e^- \rightarrow LnO^- \quad (5)$$

Density functional calculations for several $LnO^+/LnO/LnO^-$ monoxide series were done to supplement and support the

TABLE 7: Product Absorptions (cm^{-1}) Observed for Laser-Ablated Lu Atoms in Solid Argon at 10 K

$^{16}O_2$	$^{18}O_2$	$^{16}O_2 + ^{18}O_2$	$^{16}O_2 + ^{16}O^{18}O + ^{18}O_2$	R(16/18)[a]	anneal.[b]	ident.
	1466	1554, 1466	1554, 1511, 1467	1.060	b+	(OO)Lu$_x$
1100.2	1038.3	1100.1, −	1100.3, 1069.8, −	1.0596	a0−	(O$_2$)Lu$_x$
867.9	823.0	867.8, 823.0	867.9, 822.8	1.0546	a− −*	LuO$^+$ site
864.9	819.9	864.9, 819.8	864.9, 819.8	1.0549	a− −*	LuO$^+$
829.3	786.2	829.2, 786.0	829.2, 786.0	1.0548	a− −(−)	LuO
826.6	783.7			1.0547	a+ −(−)	LuO site
823.7	780.9	−, 780.7		1.0548	a− −(−)	LuO site
819.9	777.2	−, 777.0		1.0549	a− −(−)	LuO site
816.0	770.9			1.0585	b+	Lu$^+$O$_3^-$
794.0	752.7	794.0, 752.5	794.0, 752.5	1.0549	a+ −(−)	(O$_2$)LuO
755.1	713.5	755.0, 735.3, 713.5 (2:1:2)	755.1, 735.5, 713.6 (1:2:1)	1.0583	a+ +*	?
720.6	680.3	719, 679	720, 698, 679	1.059	a0−(+)	?
626.9	595.6			1.0526	a+ −(−)	LuO$_2^-$ ν_3
624.8	593.5			1.0527	a− −(W+)(Hg−)**	LuO$_2^-$ ν_3 site
570.7	542.2	570.7, 542.2		1.0526	a+ −(−)*	?
569.6	540.4			1.0540	a− −**	(LuO)$_2$ B$_{2u}$ tentative
564.5	535.3			1.0545	a+ −(+)**	(OO)$_x$(LuO)$_2$ B$_{2u}$
558.9	529.9			1.0547	a− −(W+) (Hg−)**	(OO)$_x$(LuO)$_2$ B$_{2u}$
549.2	520.9	549.2, 531.5, 521.0	549.2, 531.5, 521.0	1.0543	a+ −(+)**	(OO)$_x$(LuO)$_2$ B$_{2u}$
534.0	507.9	−, 507.7		1.0514	a+ −(+)	?
491.5	466.7	491.4, 466.7		1.0531	a+ −(+)	?
478.5	455.0			1.0516	a+ −	?

[a] Ratio (16/18) isotopic frequencies. [b] Annealing behavior: "a" denotes presence on deposition, "+, −, or 0" indicates the direction of growth in two successive annealings, "b" denotes appearance on the first annealing and "+, −, or 0" indicates changes on the second annealing, "+ or −" indicates changes on photolysis, "c" denotes appearance on photolysis, "*" indicates an increase with CCl_4 on deposition, and "**" indicates a decrease with CCl_4 on deposition.

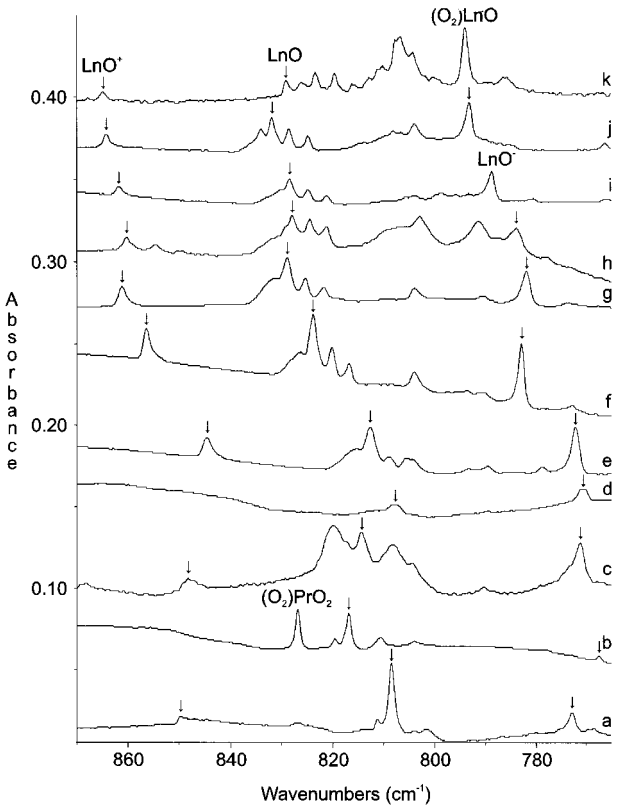

Figure 1. Infrared spectra in the 870−765 cm^{-1} region for laser-ablated lanthanide atoms co-deposited with $^{16}O_2$/Ar after 1 h deposition: (a) Ce + 1% $^{16}O_2$/Ar; (b) Pr + 1% $^{16}O_2$/Ar; (c) Nd + 0.5% $^{16}O_2$/Ar; (d) Sm + 1% $^{16}O_2$/Ar; (e) Gd + 1% $^{16}O_2$/Ar; (f) Tb + 1% $^{16}O_2$/Ar; (g) Dy + 1% $^{16}O_2$/Ar; (h) Ho + 1% $^{16}O_2$/Ar; (i) Er + 1% $^{16}O_2$/Ar; (j) Tm + 1% $^{16}O_2$/Ar; (k) Lu + 1% $^{16}O_2$/Ar. Generic Ln labels are employed; arrows denote this species for the given lanthanide metal.

experimental observations.[38] Sample molecules were chosen which simplify the calculations by minimizing the multiplicity of states and taking advantage of the special stability accorded half-filled and filled metal 4f shells. The representative calculations span the lanthanide series, showing a small but consistent decrease in bond length and increase in vibrational frequency from CeO to GdO to LuO, except for EuO, which has a longer bond length and lower frequency because of its different orbital structure due to the stability of the metal f^7 electronic configuration (Table 8). These small changes in bond length and vibrational frequency mirror the experimental results, which show an overall increase in vibrational frequency, and provide an example of the effects of lanthanide contraction.

The assigned order and spacing of the ions and neutrals of the lanthanide monoxides in the infrared spectra are consistent with the ligand field model as applied to these species and with the values provided by the calculations, although the calculations overestimate the spacing between the cation, the neutral, and the anion. The metal valence of the lanthanide ions is derived from the anticipated change in valence due to the addition or removal of an electron from the neutral species, for which the valence is known,[11,17,21] and is consistent with the ground-state multiplicities calculated for each species.

The metal 6s orbital is the most likely to gain or lose an electron for all LnO species except for EuO and YbO, which have an unoccupied metal 6s orbital. Because the 6s orbital has a radius greater than the bond length, changes in its occupation have only a small effect on the vibrational frequency, but changes in the metal 4f occupation precipitate much larger alterations in the vibrational frequency because the extension of the 4f orbitals does not exceed the bond length,[21] and so these orbitals have a greater impact on the electrostatic attraction between the Ln and the O ligand. This model is verified experimentally by the observation that the difference between the YbO and YbO$^+$ and the EuO and EuO$^+$ species, which have the 4f ^{N} configuration, is about 3 times as great as the difference between the neutral and cation of the other lanthanide monoxides, which have the 4f $^{N-1}$s configuration.

TbO Species. Upon deposition of laser-ablated Tb atoms and ions with molecular O_2 in excess argon, TbO neutral, TbO$^+$, and TbO$^-$ are all formed and trapped within the argon matrix (Figure 2). TbO neutral is observed at 823.9 (781.4) cm^{-1} in agreement with previous assignments.[7,13,14] TbO$^+$ and TbO$^-$ are observed at 856.5 (812.2) and 782.9 (742.5) cm^{-1}, respectively, and all are of comparable intensity. The isotopic frequency ratios of the above peaks are consistent with the monoxide harmonic

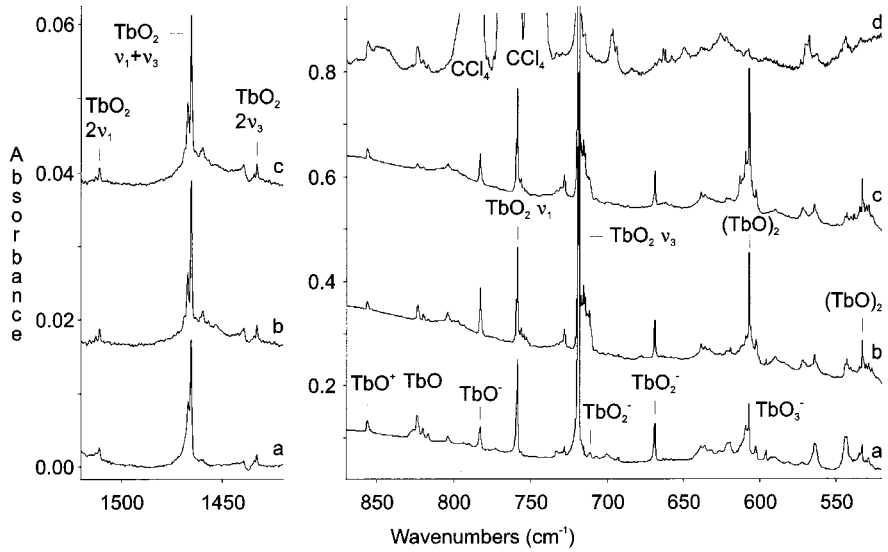

Figure 2. Infrared spectra in the 1520−1420 and 870−520 cm^{-1} regions for laser-ablated terbium atoms co-deposited with 1% $^{16}O_2$/Ar after: (a) 1 h deposition; (b) 25 K annealing; (c) 20 min Hg full arc photolysis; and (d) Tb + 0.7% $^{16}O_2$/0.01% CCl_4 in the 870−520 cm^{-1} region after 45 min deposition.

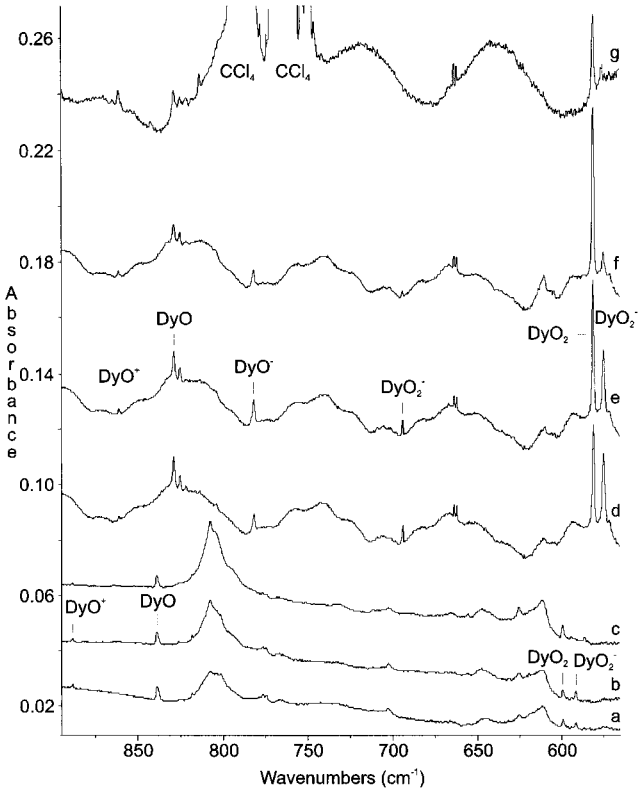

Figure 3. Infrared spectra in the 895−565 cm^{-1} region for laser-ablated dysprosium atoms co-deposited with: (a) 0.4% $^{16}O_2$/Ne after 1 h deposition with lowest laser power; (b) 0.4% $^{16}O_2$/Ne after 15 min tungsten lamp photolysis; (c) 0.4% $^{16}O_2$/Ne after 15 min Hg full arc photolysis; (d) 1% $^{16}O_2$/Ar after 1 h deposition with low laser power; (e) 1% $^{16}O_2$/Ar after 10 min tungsten lamp photolysis; (f) 1% $^{16}O_2$/Ar after 10 min Hg full arc photolysis; (g) 1% $^{16}O_2$/0.01% CCl_4: Ar after 1 h deposition with low laser power. Note the shifts between neon and argon matrixes.

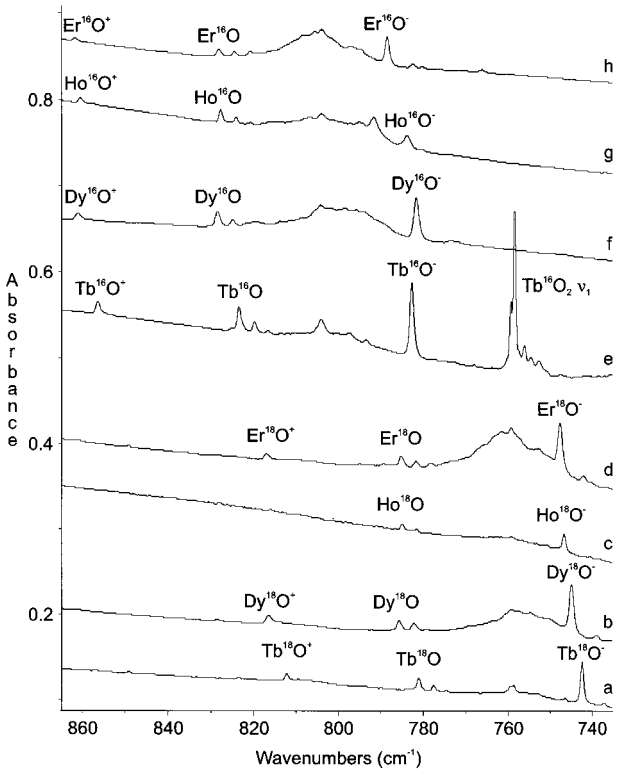

Figure 4. Infrared spectra in the 865−735 cm^{-1} region for laser-ablated lanthanide atoms after 25 K annealing: (a) Tb + 1% $^{18}O_2$/Ar; (b) Dy + 1% $^{18}O_2$/Ar; (c) Ho + 1% $^{18}O_2$/Ar; (d) Er + 1% $^{18}O_2$/Ar; (e) Tb + 1% $^{16}O_2$/Ar; (f) Dy + 1% $^{16}O_2$/Ar; (g) Ho + 1% $^{16}O_2$/Ar; (h)Er + 1% $^{16}O_2$/Ar.

ratio of 1.0548 (Table 1). Annealing to 25 K doubles the anion concentration at the expense of the other two; UV photolysis enhances the cation and decreases both the neutral and the anion. Subsequent higher temperature annealings decrease all three species. Introduction of CCl_4 dopant to reaction mixtures increased the cation relative to the neutral, but assessment of its effect on TbO^- was prevented by the strong CCl_4 absorptions.

DyO Species. DyO is observed upon deposition at 829.0 (786.1) cm^{-1}, DyO^+ at 861.2 (816.5) cm^{-1}, and DyO^- at 782.0 (745.1) cm^{-1}. Although the neutral and the cation exhibit ordinary monoxide oxygen isotopic ratios, an irregularity exists in the ratio for the DyO^- anion. The monoxide anion absorptions are located in the expected position (Figures 1 and 3), and exhibit the proper isotopic splitting, showing two isotopic peaks for both mixed and scrambled oxygen samples, but the $^{16}O/^{18}O$ isotopic ratio, 1.0495, is uncharacteristically low. Because it is

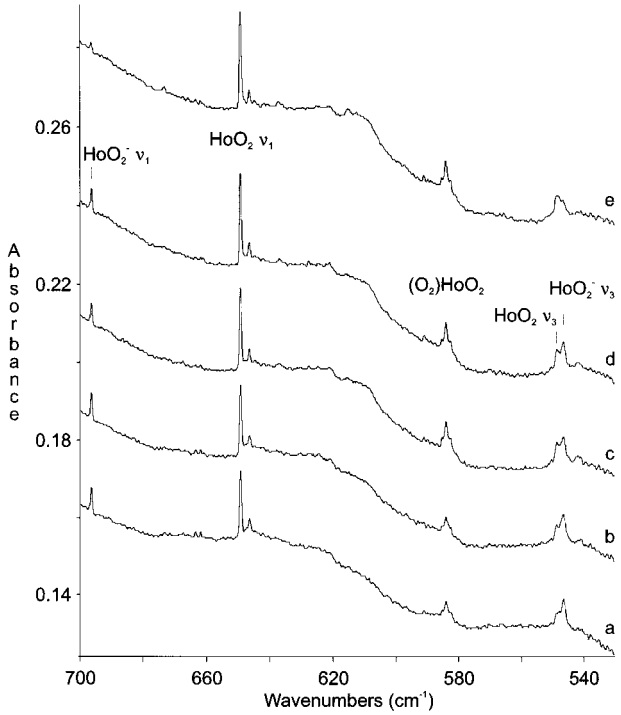

Figure 5. Infrared spectra in the 700−530 cm^{-1} region for laser-ablated holmium atoms co-deposited with 0.5% $^{16}O_2$/Ar: (a) after 1 h deposition; (b) after 25 K annealing; (c) after 17 min tungsten lamp photolysis; (d) after 30 K annealing; (e) after 10 min Hg full arc photolysis.

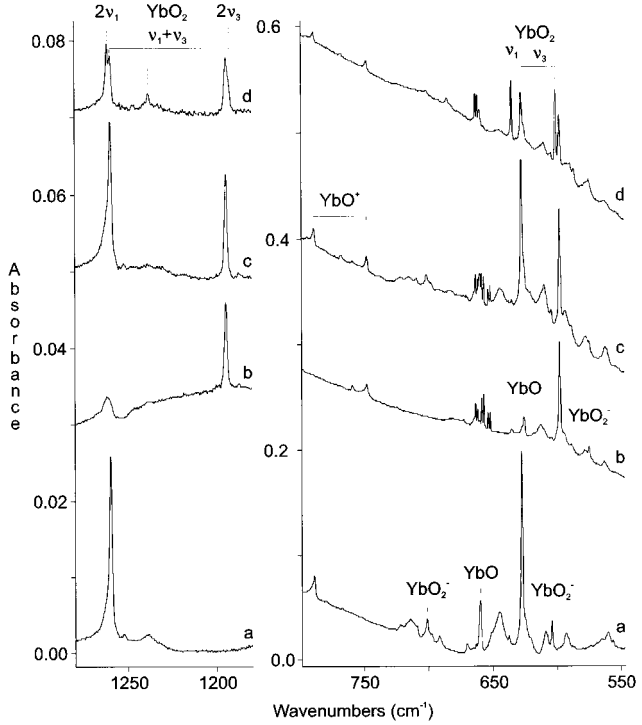

Figure 6. Infrared spectra in the 1280−1180 and 795−550 cm^{-1} regions for laser-ablated ytterbium atoms co-deposited with: (a) 1% $^{16}O_2$/Ar after 1 h deposition; (b) 1% $^{18}O_2$/Ar after 1 h deposition; (c) 2% mixed O_2/Ar after 1 h deposition; (d) 2% scrambled O_2/Ar after 1 h deposition.

known that the electronic manifold of the lanthanide oxides in general contain an abundance of low-lying states, and such a state for DyO has been measured at about 770 cm^{-1},[8] the unusually low isotopic ratio of DyO^-, 1.0495, is attributed to a perturbation of the $Dy^{16}O^-$ vibrational fundamental by a low-lying electronic state of the anion. The 36.9 cm^{-1} red shift of the DyO^- frequency upon isotopic ^{18}O substitution diminishes the perturbation for the $Dy^{18}O^-$ anion. Figure 4 shows that both $Dy^{16}O^-$ and $Ho^{16}O^-$ are perceptibly red shifted relative to their expected positions given the observed trend in the $Ln^{18}O^-$ vibrations to higher frequencies moving across the lanthanide row. The band attributed to DyO^- is diminished in the presence of CCl_4, characteristic of anionic species. Both DyO^+ and DyO neutral have also been identified in solid neon and are listed in Table 2 at 888.6 (842.3) and 839.0 (795.8) cm^{-1}, respectively.

HoO Species. HoO neutral is assigned at 828.1 (785.2) cm^{-1}, while HoO^+ absorbs at 860.5 (816.1) cm^{-1}, and HoO^- at 783.6 (746.6) cm^{-1}; the cation and the neutral have also been identified in neon at 887.9 (841.9) and 838.1 (794.6) cm^{-1}, respectively (Table 3). The anion could not be determined in neon, as the region is obscured by the intense metal ozonide band. As with DyO^-, the monoxide anion has a $^{16}O/^{18}O$ isotopic ratio that is too low. Low-lying electronic states of HoO neutral have been measured at about 610 and 840 cm^{-1},[9] which makes it reasonable that an electronic state of HoO^- could be close enough in energy to 785 cm^{-1} to perturb the vibrational frequency of $Ho^{16}O^-$ down a few cm^{-1} (Figure 4g). $Ho^{18}O^-$ can be observed in the $^{18}O_2 + CCl_4$ experiments, and although this region of the spectrum is complicated by CCl_4 sites which are on the same intensity scale as the product peak, comparison of the $^{18}O_2$ spectra with the $^{18}O_2 + CCl_4$ and the $^{16}O_2 + CCl_4$ spectra demonstrate that the $Ho^{18}O^-$ intensity is definitely diminished in the CCl_4 experiment, while the HoO^+ band intensifies.

ErO Species. The ErO system is similar to the TbO system, and the oxygen isotopic ratio of ErO^- is 1.0548, which is consistent with its identification. ErO neutral absorbs at 828.5 (785.5) cm^{-1} in accord with previous observations.[10,13] The fundamental of ErO^+ appears at 861.8 (817.0) cm^{-1} and decreases with annealing of the matrix, but increases with Hg arc photolysis at the expense of the anion, at 788.8 (747.8) cm^{-1}, and the neutral (Table 4). The anion is increased by initial annealing, but reduced by photolysis and later annealings. The oxygen isotopic ratios of 1.0548 for the ions and 1.0547 for the neutral are in mutual agreement with the harmonic oscillator ratio of 1.0551 for the ErO diatomic molecule allowing for the anharmonicity of the system. ErO^+ increases by 150% relative to ErO neutral when CCl_4 is present, and comparison of the $^{16}O_2 + CCl_4$ spectra with the $^{18}O_2 + CCl_4$ spectra in this region showed no sign of the $Er^{18}O^-$ absorption, so it is concluded that ErO^- is inhibited by CCl_4.

TmO Species. The TmO spectra resemble spectra of the other monoxides with the neutral observed at 832.0 (788.9) cm^{-1} and the cation at 864.2 (819.3) cm^{-1}. However, the lowest of the three bands, 793.2 (752.0) cm^{-1}, assigned to the monoxide anion in spectra with previous metals, is instead identified as a complexed (O_2)TmO species in this case (Table 5 and Figure 1). The cation is increased in the presence of CCl_4, which is diagnostic for this species. Oxygen-complexed TmO is increased by tungsten lamp photolysis and decreased by Hg arc photolysis but appears to be unaffected by the presence of CCl_4. The absorptions become observable in CCl_4 experiments following annealing to 25 K, but the proximity to the strong CCl_4 absorptions makes comparison of peak intensities with undoped experiments uncertain. Because these peaks do not decline upon introduction of CCl_4 to the samples, they are assigned to (O_2)TmO rather than TmO^-, since the diagnostic for an anionic species has not been met. This is not entirely unexpected as LaO shows similar behavior, forming the (O_2)MO

TABLE 8: Calculated Parameters (ADF 2.1) for CeO, EuO, GdO, and LuO Species

molecule	metal valence	multiplicity	bond length (Å)	energy (eV)	freq (cm^{-1})	intensity (km/mol)	exptl (cm^{-1})
CeO^+	f^1	doublet	1.78	−6.061	885.4	170	849.4
CeO	f^1s^1	triplet	1.82	−11.654	820.2	220	808.3
CeO^-	f^1s^2	doublet	1.85	−12.790	744.5	90	772.8
EuO^+	f^6	heptet	1.80	−9.845	758.0	90	756.9
EuO	f^7	octet	1.86	−16.281	724.7	230	667.8
EuO^-	f^8 or f^6s^2	heptet	1.90	−17.095	677.6	200	
GdO^+	f^7	octet	1.77	−13.628	888.1	140	844.8
GdO	f^7s^1	nonet	1.81	−19.959	822.5	170	812.7
GdO^-	f^7s^2	octet	1.85	−20.989	768.4	150	772.2
LuO^+	f^{14}	singlet	1.76	−2.419	888.1	70	864.9
LuO	$f^{14}s^1$	doublet	1.80	−9.555	822.7	100	829.3
LuO^-	$f^{14}s^2$	singlet	1.84	−11.083	767.4	130	

TABLE 9: Comparison of Average Argon Matrix Frequencies (cm^{-1}) for LnO_2 and LnO_2^- [a]

Ln	LnO	LnO_2	angle[b]	LnO_2^-	angle[b]	Δ ($LnO_2 - LnO_2^-$)
Ce	808.3	747.0	139°	687.0	140°	+60.0
Pr	816.9	713 ± 5	180°	659.4	157°	+54
Nd	814.2	689 ± 5	180°	667 ± 5	121°	+22
Sm	807.4	623 ± 5	180°	626.0	121°	−3
Eu	667.8		90°	610.9	129°	
Gd	812.7		97°	637.7	120°	
Tb	823.9	738.6	125°	690.1	137°	+48.5
Dy	829.0	597 ± 5	180°	634.3		−37
Ho	828.1	599.0	125°[c]	621.7		−22.7
Er	828.5			657.9	127°	
Tm	832.0	661.2	128°		133°	
Yb	660.0	630 ± 5	180°	652.7	142°	−23
Lu	829.3				124°	

[a] Average is $(\nu_1 + \nu_3)/2$. [b] Angles are upper limits estimated from oxygen 16/18 isotopic ratio for ν_3; the true bond angle for bent species is probably 5° lower. [c] Estimated from oxygen 16/18 isotopic ratio for ν_1.

analogue, but with obvious O_2 stretching counterparts,[46] whereas the O_2 vibration of the (O_2)TmO species is too weak to observe.

YbO Species. YbO^+ absorbs at 788.7 (747.8) cm^{-1} and YbO absorbs at 660.0 (625.8) cm^{-1} (Table 6). YbO^- is not observed, analogous to the EuO system as detailed in the previous lanthanide oxide publication.[28] Like EuO^+, the frequency of YbO^+ is higher than that of YbO by a greater margin than usual due to the $4f^N$ electronic configuration of the neutral monoxides of Eu and Yb as opposed to the $4f^{N-1}s$ configuration of the other lanthanide monoxides.[11,17,21]

LuO Species. The lutetium monoxide products follow the same pattern observed for the TmO absorptions, providing the fundamental of the neutral monoxide at 829.3 (786.2) cm^{-1}, the fundamental of LuO^+ at 864.9 (819.9) cm^{-1}, and the fundamental of the (O_2)LuO complex at 794.0 (752.7) cm^{-1} (Table 7 and Figure 1). Like the (O_2)TmO analogue, (O_2)LuO is increased with tungsten lamp photolysis and decreased by the Hg arc and increases upon initial annealings, but diminishes with subsequent annealing. The failure of CCl_4 to significantly affect the 794.0 (752.7) cm^{-1} absorption precludes the anionic assignment and makes the complexed species a more likely candidate.

Dioxides. Five neutral dioxides and seven dioxide anions are observed in the last seven lanthanide oxygen systems reported here, and one dioxide cation is tentatively identified. To the extent that vibrational frequencies are dependent on bond strength, an overall picture of the bond variation in the dioxides and their anions can be determined by comparison of the averages of the ν_1 and ν_3 fundamentals (Table 9). It is interesting to note that early in the lanthanide series the average frequency of the neutral dioxides is greater than that of the anions; however, later in the series, this situation is reversed and the anions possess higher frequencies and presumably stronger bonds. In all cases, the neutral monoxide frequencies exceed both dioxide frequencies, which is expected as the monoxides can doubly bond to oxygen while the dioxide bond orders lie between one and two.[26]

It is postulated that the observed trend in neutral to anion bond strength can be explained by reference to the sum of the first four ionization potentials of the metal. The sum of the first four IP's of the early lanthanide dioxides and of Tb is less than 80 eV, while the others have sums greater than 80 eV.[49] Stronger neutral dioxide bonds result in the former group, and weaker, electron-deficient bonds in the latter. An additional electron for CeO_2, PrO_2, NdO_2, and TbO_2 is therefore accommodated at the 4f level, which lowers the charge on the metal center and thus weakens the ionic bonding to the O ligands. For the others, the additional electron is accepted by the electron-deficient bonding orbitals of the neutral dioxide and participates in bonding, increasing the average vibrational frequency of the molecule.

Angles of the OLnO molecules are estimated from the oxygen isotopic ratio of the ν_3 fundamentals ($Ln^{16}O_2/Ln^{18}O_2$) in the harmonic oscillator approximation.[50] Introduction of error because of the uncertainty of the frequency measurements (±0.1 cm^{-1}) causes an uncertainty in the isotopic ratio of ±0.0004. The harmonic frequency ratio, obtained from analysis of the observed ν_3 and $2\nu_3$ modes of TbO_2, introduces an additional correction of about +0.0002 to the observed ratio, because bond angles calculated with observed anharmonic frequencies are upper limits for the true angle.

OTbO Species. In agreement with previous authors, the ν_1 and ν_3 vibrational fundamentals of TbO_2 are observed at 758.6 (718.6) and 718.6 (683.2) cm^{-1}, respectively.[13,14] In addition, a complete set of overtone and combination bands is observed (Figure 2). The $\nu_1 + \nu_3$ combination band absorbs prominently at 1465.5 (1391.5) cm^{-1}, the $2\nu_1$ overtone at 1510.9 (1431.9) cm^{-1}, and the $2\nu_3$ overtone at 1433.0 (1362.5) cm^{-1} (Figure 2 and Table 1). The anharmonicity associated with these peaks is 11.7 (10.4), 6.3 (5.5), and 4.2 (3.9) cm^{-1}, respectively. The bond angle upper limit, derived from the oxygen isotopic ratio for the ν_3 modes,[50] 1.0518, is 125°; the frequency uncertainty introduces an error of ±0.0004 in this ratio which corresponds to ±5°. The harmonic frequency ratio, deduced from ν_3 and $2\nu_3$, 1.0520, predicts an angle of 122° which the same ±5° uncertainty. Upon annealing, the ν_1 and ν_3 absorptions of TbO_2 shift to 752.7 (713.1) and 711.6 (676.3) cm^{-1}, respectively, and these absorptions track with bands near 1100 cm^{-1} assigned in Table 1 to the O−O vibrations of the O_2 complexed dioxide molecule.

The ν_3 fundamental of TbO_2^- has been observed at 669.0 (636.5) cm^{-1} and the ν_1 at 711.2 (673.2) cm^{-1}, which provides an upper limit of 137° for the bond angle based on the ν_3 oxygen

isotopic ratio of 1.0511.[50] Both of these bands present oxygen isotopic doublets in mixed oxygen and triplets in scrambled oxygen experiments, indicating that the dioxide anions are formed by acquisition of an electron by the dioxide neutral. Doping of the reactant gas with CCl_4 cuts the concentration of TbO_2^- significantly relative to the concentration of the neutral dioxide, supporting the assignment to an anionic species (Figure 2).

ODyO Species. The ν_3 fundamental of DyO_2 is observed at 580.5 (553.3) cm^{-1} in argon and 599.2 (571.3) cm^{-1} in neon; for the isotopically substituted $^{16}ODy^{18}O$ molecule in argon, the ν_1 is additionally observed at 607.5 cm^{-1}. Because the $\nu_1 + \nu_3$ combination band has been identified at 1189.4 (1128.0) cm^{-1}, the ν_1 fundamental of the $Dy^{16}O_2$ ($Dy^{18}O_2$) molecule can be estimated at 612.2 (578.0) cm^{-1}, which provides an oxygen isotopic ratio of 1.0592. The ν_3 oxygen isotopic ratio, 1.0492, is lower than the calculated harmonic oscillator ratio, 1.0500, which is an indicator of a linear molecule, as is the ν_1 ratio of 1.0592.[50] It is interesting to note that the $2\nu_1$ mode is also observed for the $^{16}ODy^{18}O$ molecule with 22% of the intensity of the $\nu_1 + \nu_3$ counterpart. In contrast to the previously identified linear lanthanide dioxides, the ν_1 mode is observed at a higher frequency than the ν_3 mode.

Both the ν_1 and ν_3 fundamentals of the DyO_2^- anion are observed in argon at 693.9 (656.9) and 574.6 (548.5) cm^{-1}, respectively (Figure 3). These bands are less intense relative to the neutral molecule absorptions in high laser power experiments and those containing CCl_4 and decrease with Hg arc photolysis. The ν_3 fundamental of DyO_2^- in neon absorbs at 591.2 (564.1) cm^{-1}, is nearly as intense as that of the neutral on deposition, and is increased following tungsten lamp photolysis, but completely destroyed by the Hg arc (Figure 3). As an impurity in hydrogen experiments, the DyO_2^- anion is about twice as intense as the DyO_2 neutral absorption. These fundamentals exhibit the characteristic doublet in experiments using mechanically mixed oxygen samples and triplet with statistically scrambled oxygen samples, indicative of a dioxide species. The positions of the fundamentals are familiar, as they fall very near those of SmO_2^-, EuO_2^-, and GdO_2^-. The isotopic ratio of the ν_3 fundamental is, however, lower than expected at 1.0476 in argon and 1.0480 in neon, even lower than the ratio of the linear neutral molecule, 1.0492, although this molecule is assigned a C_{2v} symmetry based on the presence of the ν_1 fundamental. The deviation in the oxygen isotopic ratio from the expected value is attributed to unusual stretch−stretch interactions and anharmonicity in the vibrations.

Annealing after photolysis gives rise to a very weak band at 547.6 cm^{-1}, the same position as the dioxide anion, which is destroyed by the Hg arc. Because the ν_1 fundamental of the anion does not return, this weak band at the same frequency as the anion, but broader, is due to a different species. It tracks with a band of comparable intensity at 1107.8 cm^{-1}, and the two are due to the oxygen-complexed neutral dioxide species, $(O_2)DyO_2$. The 547.6 cm^{-1} band is very weak and is obscured in most isotopic experiments by the anion, so it is not reported in Table 2.

OHoO Species. Absorbing at 649.2 (613.5) cm^{-1} in argon and 668.2 (631.1) cm^{-1} in neon, the ν_1 of HoO_2 is the dominant product peak in the Ho + O_2 spectra, unlike the usual case, where ν_3 is much more intense than ν_1 (Figure 5). The ν_3 fundamental absorbs at 548.8 (522.7) cm^{-1} in argon, but could not be identified in neon. Both absorptions increase with initial annealing and photolysis, although the ν_3 fundamental is more difficult to track because it overlaps with a nearby product peak. In contrast to thermal Ho atom experiments,[9b,c] the lack of photoaggregation is due to the presence of dioxygen, which consumes any unreacted Ho atoms. In argon with mixed and scrambled oxygen samples, respectively, the ν_1 fundamental shows an oxygen isotopic doublet and a triplet; the ν_3 fundamental, however, is significantly broadened by overlap with the adjacent peak and is nearly indiscernible with mixed and scrambled oxygen isotopes. The molecule must be bent because the ν_1 fundamental is strongly observed and suggests an angle of approximately 125°.

The interfering peak adjacent to the HoO_2 ν_3 fundamental is the ν_3 fundamental of the HoO_2^- anion. The ν_1 fundamental is observed at 696.2 (659.1) cm^{-1} and is as intense as the ν_3, 547.2 (520) cm^{-1}, but is not overlapped and is therefore more distinct. Both modes decrease together on annealing and are destroyed by Hg arc photolysis and CCl_4 dopant. Because the isotopic ratios for both the ν_1 and ν_3 fundamentals of the anion fall between the ratios of the ν_1 and ν_3 fundamentals of the neutral, the anion is more bent than the neutral.

A tentative assignment is made to the HoO_2^+ cation at 644.9 (614.9) cm^{-1}. This species clearly shows an isotopic triplet in the scrambled oxygen sample and appears after Hg arc photolysis, although it does not increase in the presence of CCl_4, so this assignment is less certain. The oxygen isotopic triplet of peaks and the ν_3 isotopic ratio of 1.0488 predict that this species is a linear dioxide. The same species absorbs in neon at 657.9 (627.6) cm^{-1}, also appearing on photolysis, with an isotopic ratio of 1.0483 (Table 3).

A final isotopic set of peaks attributed to an HoO_2 species appears at 583.9 (556.3) cm^{-1} and is enhanced by annealing. Although it cannot be tracked with an O−O stretch, it is conjectured that this absorption is due to a blue-shifted O_2 complex of the neutral HoO_2 molecule (Figure 5). The isotopic ratio of 1.0496 is close to the HoO_2 linear harmonic ratio of 1.0502, and this band appears between the ν_3 fundamentals of HoO_2 and HoO_2^+, as was also true for the $(O_2)PrO_2$ species reported in the earlier paper.[28] The increase with annealing supports assignment to an oxygen complex; the absence of an assignment to the ligated O_2 molecule does not preclude such an identification, as the latter mode is weak.

OErO Species. The ν_1 and ν_3 absorptions of ErO_2^- occur at 702.3 (665.0) and 613.4 (583.0) cm^{-1}, respectively (Table 4). An upper limit of 127° is provided for the bond angle from the ν_3 oxygen isotopic ratio.[50] The fundamentals decline with annealing of the matrix and are completely eliminated by Hg arc photolysis. In samples doped with CCl_4, the intensities of the ErO_2^- absorptions are down by 80% relative to the yield of neutral ErO. Other erbium dioxide species could not be identified. ErO_2^- is also present as an impurity in Er + N_2 experiments.

OTmO Species. The ν_3 absorption of TmO_2 occurs at 615.7 (585.2) cm^{-1} and the ν_1 at 706.6 (668.9) cm^{-1} (Table 5). Like isoelectronic ErO_2^-, the oxygen isotopic ratio of 1.0521 provides a bond angle upper limit of 128°,[50] as opposed to the case presented for the CeO_2^-/PrO_2 and PrO_2^-/NdO_2 pairs, which have different geometries, although the electron count is the same within each pair.[28] The ν_1 and ν_3 fundamentals for $Tm^{16}O_2$ are found as an impurity in Tm + H_2 and Tm + N_2 experiments, which provide very dilute $^{16}O_2$ data. It is noted that the TmO_2 neutral ν_1 and ν_3 absorptions are, respectively, 4.3 (3.9) and 2.3 (2.2) cm^{-1} higher than the fundamentals of ErO_2^-. Because the molecules are isoelectronic, two primary factors that affect the differences in the vibrational frequencies are the increase in the mass of the metal atom and of the nuclear charge upon

substituting Tm for Er. These two factors work in opposite directions, the greater nuclear mass causing a decrease in the vibrational frequency, but offset by an increase due to the stronger attraction of the metal center to the O ligands because of the greater nuclear charge. The net effect is the observed small shift to higher frequency for the TmO_2 neutral.

Tentatively, the TmO_2^- ν_3 absorption is assigned at 613.1 (582.9) cm^{-1}. It is very weak in high-power experiments, but much stronger in low-power experiments, approaching neutral TmO_2 in intensity. Because, like the dioxide anions of dysprosium and holmium, this band is decreased with Hg arc photolysis and eliminated with CCl_4 and is located in the same proximity relative to its neutral counterpart, the 613.1 cm^{-1} band is probably due to the TmO_2^- anion, but lacking clear scrambled oxygen isotopic confirmation, the assignment is tentative.

OYbO Species. Molecular YbO_2 is observed in solid argon at 627.7 (597.9) cm^{-1}, and the $\nu_1 + \nu_3$ combination band absorbs at 1259.8 (1194.7) cm^{-1} (Table 6). The ν_3 oxygen isotopic ratio of YbO_2, 1.0498, is appropriate for a linear molecule, and the ν_1 fundamental is observed only for the isotopically substituted $^{16}OYb^{18}O$ molecule at 635.0 cm^{-1} (Figure 6). In addition to the combination band for the $^{16}OYb^{18}O$ molecule at 1238.2 cm^{-1}, the $2\nu_1$ and $2\nu_3$ overtones are observed at 1261.7 and a shoulder at 1193 cm^{-1}, respectively (Figure 6). Because the ν_1 and ν_3 modes of the $^{16}OYb^{18}O$ molecule are of different symmetry than those of the $^{16}OYb^{16}O$ and $^{18}OYb^{18}O$ molecules, interactions between the modes are altered from the pure oxygen isotopic case, which explains the appearance of the $2\nu_1$ and $2\nu_3$ overtones for the $^{16}OYb^{18}O$ molecule and the weak intensity of the combination band, which is shifted 2.5 cm^{-1} *higher* than the sum of the contributing fundamentals, due to a positive quartic term in the anharmonic potential for the linear $^{16}OYb^{18}O$ molecule, interaction with the $2\nu_1$ and $2\nu_3$ modes, or both. Without accounting for the anharmonicity of the motions, the ν_1 mode is estimated, $(\nu_1 + \nu_3) - \nu_3$, at 632.1 (596.8) cm^{-1}, nearly coincident with the ν_3 fundamental.

Both the ν_1 and ν_3 fundamentals of YbO_2^- are observed, respectively, at 701.2 and 604.2 (574.6) cm^{-1}. The ν_1 fundamental of $^{18}OYb^{18}O^-$ is obscured by CO_2 impurity at 663.4 and 661.8 cm^{-1}. Because neither of these bands is strong, and ν_1 is even weaker than ν_3, they are difficult to track but can be plainly observed as an impurity in Yb + N_2 and Yb + H_2 experiments, which have only trace quantities of oxygen and therefore do not contain broad bands due to ytterbium oxide aggregates. These experiments clearly link the two absorptions, and the oxygen experiments provide the isotopic components. The $^{16}O_2/^{18}O_2$ isotopic ratio of the ν_3 fundamental is 1.0515, which provides an upper limit for the bond angle of 142°.[50]

OLuO Species. The ν_3 fundamental of LuO_2^- anion absorbs at 626.9 (595.6) cm^{-1} in solid argon and has a satellite at 624.8 (593.5) cm^{-1} (Table 7). This absorption is cut by more than 50% relative to the neutral monoxide in CCl_4 doped samples. It is too weak to be observed in mixed and scrambled oxygen samples, but is present in Lu + H_2 experiments, which makes it likely that the observed band is due to a simple oxide. The oxygen isotopic ratio of 1.0526 yields an upper limit of 124° for the bond angle.[50]

Trioxide Anions. Only TbO_3^- could be identified in the second half of the lanthanide series. It can be modeled after the example of PrO_3^- provided in the earlier paper.[28]

TbO_3^-. The absorption at 596.1 (566.7) cm^{-1} is tentatively assigned to the TbO_3^- trioxide anion. In mixed $^{16}O_2 + {}^{18}O_2$ samples, no intermediate peaks could be determined, but following the example of PrO_3^-, the two intervening peaks for this molecule are in this case too weak to rise above the noise level of the mixed sample.[28] The 596.1 (566.7) cm^{-1} absorption is in an appropriate location for the trioxide anion; furthermore, the band decreases with Hg arc photolysis and is eliminated upon introduction of CCl_4 into the reaction mixture, which is strongly suggestive of anionic behavior. Moreover, low laser power experiments (low metal concentration) decisively favor this absorption over the nearby 607.2 cm^{-1} peak, which is assigned to $(TbO)_2$. This observation indicates that the 596.1 (566.7) cm^{-1} absorber has a higher O/Ln ratio than $(TbO)_2$ and is consistent with a high oxygen content species. Like PrO_3^- this molecule has an oxygen isotopic ratio near that of the dioxide (bent at about 120°), which suggests that the TbO_3^- anion may be planar with D_{3h} symmetry.[28]

$(LnO)_2$ Rings. A dimetal dioxide ring of D_{2h} or C_{2v} symmetry has been observed in five of the last seven lanthanide systems. The ring forms both through dimerization of the monoxide molecule and through addition of a second metal atom to a metal dioxide or metal dioxygen complex.[28,51] It absorbs in the lower end of the Ln−O region of the spectrum and is favored by higher laser power relative to the metal monoxides and dioxides, supporting assignment to a higher metal species.

$(TbO)_2$. Two vibrational stretching modes of the $(TbO)_2$ ring have been observed at 607.2 (576.7) and 532.7 (505.6) cm^{-1} (Figure 2). The fundamentals increase with initial annealing and Hg arc photolysis and subsequently red-shift several wavenumbers with additional annealing, as the ring complexes molecular O_2. The oxygen isotopic ratios of the observed bands, 1.0529 and 1.0536, are both lower than the monoxide ratio of 1.0544, indicating that the ring is likely nonplanar.

$(DyO)_2$. Absorptions occurring at 609.6 (578.6) and 522.2 (495.8) cm^{-1} are assigned to $(DyO)_2$. The oxygen isotopic ratios, 1.0536 and 1.0532, are both lower than the monoxide ratios and suggest that the ring is puckered (Table 2). Because the bands present 1:1:1 isotopic triplets in mixed and 1:2:1 isotopic triplets in scrambled oxygen samples, it is evident that both direct insertion of Dy into O_2 followed by addition of atomic Dy and dimerization of DyO are instrumental in formation of this product.[28]

$(TmO)_2$. A sharp band absorbs at 553.7 (525.1) cm^{-1} with broader red-shifted peaks, the most prominent of which is at 541.3 (513.5) cm^{-1}. Because it shows an isotopic doublet in mixed oxygen samples, likely provides a triplet in scrambled oxygen samples (but cannot be determined due to complications from the isotopic components of the broader peaks), and has a ratio of 1.0545, which is the same as that of the diatomic molecule, the 553.7 (525.1) cm^{-1} absorption is assigned to the $(TmO)_2$ dimer. Since it is also observed as an oxygen impurity in Tm + H_2 and Tm + N_2 experiments, this is assigned to the uncomplexed species, while the broader red-shifted peaks, including 541.3 (513.5) cm^{-1}, which have a similar oxygen isotopic ratio and isotopic peak pattern, are assigned to the complexed $(O_2)_x(TmO)_2$ species.

$(YbO)_2$. Two bands which track together throughout photolysis and annealing cycles and are favored by higher laser power experiments are present in Yb + O_2 spectra at 590.9 (560.6) and 540.1 (512.3) cm^{-1} in solid argon. The more intense of the two absorptions, 540.1 (512.3) cm^{-1}, shows a broad isotopic triplet in scrambled oxygen samples; both show an oxygen isotopic doublet in mixed oxygen samples. Because these peaks are broad, but sharpen with annealing, they are probably due to the two modes of an O_2-ligated $(YbO)_2$ ring.

$(LuO)_2$. Multiple peaks ranging from 569.6 (540.4) to 549.2 (520.9) cm^{-1} are tentatively assigned to $(LuO)_2$ and its O_2

complexes, and the primary sites are listed in Table 7. These peaks are more prominent in high laser power experiments relative to other product peaks in the spectra, which suggests that they may be due to a species containing a greater number of metal atoms. Although mixed and scrambled oxygen isotopic components can only be identified for the lowest of the peaks and are provided in the table, the higher peaks have similar oxygen isotopic ratios and are almost certainly due to the same species with a different number of O_2 ligands.

Metal Ozonides. All seven of the metal oxide systems reported in this paper have a broad absorption in the lower 800 cm^{-1} region that is attributed to an O_3^- fundamental of the $Ln^+O_3^-$ species. This agrees with previous lanthanide ozonide assignments and the analogous alkali metal ozonide species.[28,52,53] Observation of the $Ln^+O_3^-$ species shows that the lanthanide metal atoms also have a +1 oxidation state. The $Ln^+O_3^-$ species arise from the reaction of LnO with O_2 and confirm that these are monometal species. In pure dioxygen, the same $Ln^+O_3^-$ species is observed as the only metal product, which must contain a single metal.

Other Complexes and Aggregates. Metal clusters, which form when rare gas matrices containing lanthanide metal atoms are annealed,[9b] weakly perturb molecular O_2, allowing it to absorb infrared radiation near 1552 cm^{-1} after annealing, nearly unchanged in frequency from the Raman value observed for O_2 in argon matrixes.[54] Several unidentified O−O and Ln−O stretching modes are also listed in Tables 1−7. These bands are assigned to additional molecular oxygen complexes and metal oxide aggregates, which cannot be identified from the spectral data.

Conclusions

The reaction products of laser-ablated late lanthanide metal atoms with molecular O_2 have been isolated in argon and characterized by infrared spectroscopy of isotopically substituted species. Seven new monoxide cations, four new monoxide anions, four new dioxide neutrals, and seven new dioxide anions have been identified. This concludes the current study of lanthanide oxide species and taken with the previous publication allows the recognition of trends across the lanthanide series.[28] All 13 of the neutral lanthanide monoxides discussed agree with previous matrix and gas-phase work; dioxides previously observed in matrix studies also agree with those presented here.[1−14] In addition, overtone and combination bands further confirm assignments.

At the beginning of the lanthanide series, the average frequency, and by extension, bond energy, of the dioxide neutrals exceeds that of the dioxide anions. Later in the series, this situation is reversed, with average vibrational frequencies of the anions greater than the respective neutral frequencies. This change in the order of the average vibrational frequencies tracks roughly with the sum of the first four ionization potentials of the atomic lanthanides. Metals for which the sum of the first four ionization potentials is less than 80 eV[49] have higher frequency neutral stretches, while the others have lower frequency neutral stretches and presumably electron-deficient bonds. Therefore, the vibrational frequencies of the anions of the neutrals with frequencies less than 670 cm^{-1} shift higher as their bonds are satisfied, while those with frequencies higher than 670 cm^{-1} shift lower as the anion is formed, which also decreases the electrostatic attractions within the molecules.

The lanthanide monoxides have commonly been modeled electrostatically by the ligand field.[11,17,21] The observation of increased cation and decreased anion vibrational frequencies for a given monoxide fits this model as the charge on the metal center is increased and decreased in turn. The overall migration toward higher frequencies for all monoxides with progression across the series is indicative of shorter bond lengths and demonstrates the lanthanide contraction. Both of these effects are apparent in the dioxide pairs, PrO_2/NdO_2^+, GdO_2^-/TbO_2, and ErO_2^-/TmO_2, where the number of electrons is the same and the geometry is very similar. All three pairs show a shift to higher frequency for the heavier metal due to increased electrostatic attraction and lanthanide contraction, although the net effect is small for the ErO_2^-/TmO_2 pair.

Acknowledgment. We gratefully acknowledge financial support from National Science Foundation Grant CHE 97-00116, the use of the ADF 2.1 computational package provided by E. J. Baerends and maintained by M. Neurock, and helpful correspondence with R. W. Field.

References and Notes

(1) Linton, C.; Dulick, M.; Field, R. W. *J. Mol. Spectrosc.* **1979**, *78*, 428. Linton, C.; Dulick, M.; Field, R. W.; Carette, P.; Barrow, R. F. *J. Chem. Phys.* **1981**, *74*, 189. Linton, C.; Dulick, M.; Field, R. W.; Carette, P.; Leyland, P. C.; Barrow, R. F. *J. Mol. Spectrosc.* **1983**, *102*, 441.

(2) Shenyavskaya, E. A.; Egorova, I. V.; Lupanov, V. N. *J. Mol. Spectrosc.* **1973**, *47*, 355. Dulick, M.; Field, R. W. *J. Mol. Spectrosc.* **1985**, *113*, 105.

(3) Kaledin, L. A.; Shenyavskaya, E. A.; Kovács, I. *Acta Phys. Hung.* **1983**, *54*, 189. Kaledin, L. A.; Bloch, J. C.; McCarthy, M. C.; Gurvich, L. V.; Field, R. W. *Mol. Phys.* 1994, *83*, 881.

(4) Linton, C.; Bujin, G.; Rana, R. S.; Gray, J. A. *J. Mol. Spectrosc.* **1987**, *126*, 370.

(5) McDonald, S. A. Ph.D. Thesis, Massachusetts Institute of Technology, Cambridge, MA, 1985.

(6) Yadav, B. R.; Rai, S. B.; Rai, D. K. *J. Mol. Spectrosc.* **1981**, *89*, 1.

(7) Kulikov, A. N.; Kaledin, L. A.; Kobyliansky, A. I.; Gurvich, L. V. *Can. J. Phys.* **1984**, *62*, 1855.

(8) Linton, C.; Gaudet, D. M.; Schall, H. *J. Mol. Spectrosc.* **1986**, *115*, 58.

(9) (a) Liu, Y. C.; Linton, C.; Schall, H; Field, R. W. *J. Mol. Spectrosc.* **1984**, *104*, 72. (b) Klotzbücher, W. E.; Petrukhina, M. A.; Sergeev, G. B. *J. Phys. Chem. A* **1997**, *101*, 4548. (c) Nemukhin, A. V.; Ermilov, A. Yu.; Petrukhina, M. A.; Klotzbücher, W. E.; Smets, J. *Spectrochim. Acta A* **1997**, *53*, 1803.

(10) Kaledin, L. A.; Shenyavskaya, E. A. *J. Mol. Spectrosc.* **1989**, *133*, 469.

(11) Linton, C.; McDonald, S.; Rice, S.; Dulick, M.; Liu, Y. C.; Field, R. W. *J. Mol. Spectrosc.* **1983**, *101*, 332. McDonald, S. A.; Rice, S.; Field, R. W.; Linton, C. *J. Chem. Phys.* **1990**, *93*, 7676.

(12) Bernard, A.; Effantin, C. *Can. J. Phys.* **1986**, *64*, 246.

(13) DeKock, R. L.; Weltner, W., Jr. *J. Phys. Chem.* **1971**, *75*, 514.

(14) Gabelnick, S. D.; Reedy, G. T.; Chasanov, M. G. *J. Chem. Phys.* **1974**, *60*, 1167.

(15) Van Zee, R. J.; Ferrante, R. F.; Zeringue, K. J.; Weltner, W., Jr. *J. Chem. Phys.* **1981**, *75*, 5297.

(16) Konnov, S. A.; Serebrennikov, L. V.; Mal'tsev, A. A. *Russ. J. Inorg. Chem.* **1982**, *27*, 367.

(17) Dulick, M.; Murad, E.; Barrow, R. F. *J. Chem. Phys.* **1986**, *85*, 385.

(18) Dolg, M.; Stoll, H. *Theor. Chim. Act.* **1989**, *75*, 369.

(19) Dolg, M.; Stoll, H.; Flad, H.; Preuss, H. *J. Chem. Phys.* **1992**, *97*, 1162.

(20) Wang, S. G.; Pan, D. K.; Schwarz, W. H. E. *J. Chem. Phys.* **1995**, *102*, 9296. Wang, S. G.; Schwarz, W. H. E. *J. Phys. Chem.* **1995**, *99*, 11687.

(21) Field, R. W. *Ber. Bunsen-Ges. Phys. Chem.* **1982**, *86*, 771. Dolg, M.; Stoll, H.; Preuss, H. *Chem. Phys. Lett.* **1990**, *174*, 208. Dolg, M.; Stoll, H.; Preuss, H. *Chem. Phys.* **1990**, *148*, 219.

(22) Liu, W.; Dolg, M.; Li, L. *J. Chem. Phys.* **1998**, *108*, 2886.

(23) Staley, H. G.; Norman, J. H. *Int. J. Mass. Spectrom. Ion Phys.* **1969**, *2*, 35.

(24) Ackerman, R. J.; Rauh, E. G.; Thorn, R. J. *J. Chem. Phys.* **1976**, *65*, 1027.

(25) Pupp, C.; Gingerich, K. A. *J. Chem. Phys.* **1971**, *54*, 3380. Kordis, J.; Gingerich, K. A. *J. Chem. Phys.* **1977**, *66*, 483.

(26) Heinemann, C.; Cornehl, H. H.; Schröder, D.; Dolg, M.; Schwarz, H. *Inorg. Chem.* **1996**, *35*, 2463. Cornehl, H. H.; Wesendrup, R.; Diefenbach, M.; Schwarz, H. *Chem.—Eur. J.* **1997**, *3*, 1083.

(27) Cockett, M. C. R.; Nyulászi, L.; Veszprémi, T.; Wright, T. G.; Dyke, J. M. *J. Electron Spectrosc. Relat. Phenom.* **1991**, *57*, 373 and references therein.
(28) Willson, S. P.; Andrews, L. *J. Phys. Chem. A* **1999**, *103*, 3171 (early Ln oxide).
(29) Burkholder, T. R.; Andrews, L. *J. Chem. Phys.* **1991**, *95*, 8697.
(30) Hassanzadeh, P.; Andrews, L. *J. Phys. Chem.* **1992**, *96*, 9177.
(31) Chertihin, G. V.; Saffel, W.; Yustein, J. T.; Andrews, L.; Neurock, M.; Ricca, A.; Bauschlicher, C. W., Jr. *J. Phys. Chem.* **1996**, *100*, 5261.
(32) Andrews, L.; Bare,W. D.; Chertihin, G. V. *J. Phys. Chem. A* **1997**, *101*, 8417.
(33) Huber, K. P.; Herzberg, G. *Constants of Diatomic Molecules*; Van Nostrand Reinhold: New York, 1979.
(34) Thompson, W. E.; Jacox, M. E. *J. Chem. Phys.* **1989**, *91*, 3826. Zhou, M. F.; Hacaloglu, J.; Andrews, L. *J. Chem. Phys.* **1999**, *110*, 9450.
(35) Andrews, L.; Spiker, R. C., Jr. *J. Phys. Chem.* **1972**, *76*, 3208.
(36) Chertihin, G. V.; Andrews, L. *J. Chem. Phys.* **1998**, *108*, 6404.
(37) Andrews, L.; Ault, B. S.; Grzybowaki, J. M.; Allen, R. O. *J. Chem. Phys.* **1975**, *62*, 2461.
(38) *ADF 2.1*, *Theoretical Chemistry*; Vrije Universiteit: Amsterdam.
(39) Baerends, E. J.; Ellis, D. E.; Ros, P. *Chem. Phys.* **1973**, *2*, 41.
(40) teVelde, G.; Baerends, E. J. *Comput. Phys.* **1992**, *99*, 84.
(41) Vosko, S. H.; Wilk, L.; Nusair, M. *Can. J. Phys.* **1980**, *58*, 1200.
(42) Becke, A. D. *Phys. Rev. A* **1988**, *38*, 3098.
(43) Perdew, J. P. *Phys. Rev. B* **1986**, *33*, 8822.
(44) Ziegler, T. Ph.D. Thesis, Vrije Universiteit, Amsterdam, 1987. Heinemann, C.; Cornehl, H. H.; Scroder, D.; Dolg, M.; Schwarz, S. *Inorg. Chem.* **1996**, *35*, 2463.
(45) Boerrigte, P. M. Ph.D. Thesis, Vrije Universiteit, Amsterdam, 1987.
(46) Andrews, L.; Zhou, M. F.; Chertihin, G. V.; Bauschlicher, C. W., Jr. *J. Phys. Chem. A* **1999**, *103*, 6525.
(47) Illenberger, E. *Ber. Bunsen-Ges. Phys. Chem.* **1982**, *86*, 252. Matejcik, S.; Kiendler, A.; Stamatovic, A.; Märk, T. D. *Int. J. Mass. Spectrom. Ion Process.* **1995**, *149/150*, 311.
(48) Hiraoka, K. *J. Chem. Phys.* **1988**, *89*, 3190. Celotta, R. J.; Bennett, R. A.; Hall, J. L.; Siegel, M. W.; Levine, J. *Phys. Rev. A.* **1972**, *6*, 631.
(49) Martin, W. C., Zalubas, R., Hogan, L., Eds. *Atomic Energy Levels—The Rare Earth Elements*; U.S. Dept. Commerce, Natl. Bur. Stds.: Washington, DC, 1978.
(50) Allavena, M.; Rysnik, R.; White, D.; Calder, V.; Mann, D. E. *J. Chem. Phys.* **1969**, *50*, 3399.
(51) Chertihin, G. V.; Andrews, L.; Rosi, M.; Bauschlicher, C. W., Jr. *J. Phys. Chem. A* **1997**, *101*, 9085.
(52) Kelsall, B. J. *Diss. Abstr. Int. B* **1980**, *40*, 5694.
(53) Spiker, R. C., Jr.; Andrews, L. *J. Chem. Phys.* **1973**, *59*, 1851.
(54) Andrews, L.; Smardzewski, R. R. *J. Chem. Phys.* **1973**, *58*, 2258.